



# Structural dynamics of molybdenum vanadium oxide (MoVO<sub>x</sub>)

## Influence of activation condition

Durga Devi Suppiah<sup>1</sup> · Anna Komar<sup>2</sup> · Sharifah Bee Abd Hamid<sup>1</sup>

Received: 9 August 2016 / Accepted: 18 March 2017  
© Akadémiai Kiadó, Budapest, Hungary 2017

**Abstract** Molybdenum and vanadium oxides were known to be an effective catalyst for light olefin (propane) activation for conversion to value-added chemicals. However, it is difficult to control the selectivity to desired product whereby subsequent reaction can lead to coking and rapid catalyst deactivation. One of the key ways to improve on the above limitation is to optimise and control the molybdenum phase structure, particularly during catalyst precursor activation stage. This paper demonstrates the combination of optimal *in situ* activation under different condition and thermal analysis for structural control that can help to guide and gain an insight into the structure–activity relationship of the nanostructured catalyst system. *In situ* XRD analysis reveals the crystallization of molybdenum vanadium oxide was highly influenced by the activation condition hence exhibiting different structural properties. Activation under Air at 300 °C forms highly crystalline hexagonal phase and transforms to thermodynamically stable orthorhombic ( $\text{o-MoO}_3$ ) phase at 450 °C. Activation under inert (helium) reveals the precursor remains amorphous until nanostructuring occurs at 450 °C. The precursor further transforms to the thermodynamically stable crystallized tetragonal phase ( $\text{Mo}_5\text{O}_{14}$ ) at 500 °C. The obtained structural transition information is important in order to control and identify the catalytic active phase that is suitable for a particular reaction.

**Keywords** In situ XRD · Structure · Activation · Molybdenum

## Introduction

Molybdenum oxides were identified in activating C–H bonds of alkanes, especially light olefins (propane) for selective partial oxidation. The structural complexity, the ability to occur at +4 to +6 oxidation states and oxygen coordination geometry variation of molybdenum oxides give rise to good catalytic performances. The capability to do so creates high structural diversity of the mixed transition metal oxides. Vanadium also has rich coordination geometries and oxidizing state ranging from +3 to +5. By incorporating vanadium as a promoter into the molybdenum oxide system, the desired active phase can be achieved. Catalytic activity increased with vanadium addition but less selective at iso-conversion [1–4]. The catalyst synthesis applying a ‘top down’ approach starts with a bulk solid then structurally decomposed to obtain nanostructures which are then subsequently assembled into a new bulk material [5, 6]. In order to enhance catalytic performance, studies of structure–activity relationship are essential to understand the catalyst system, especially during thermal induced activation [7]. *In situ* studies are described as a technique that gives detailed structural and chemical atomic scale insight in complex heterogeneous catalyst in order to determine the structure–activity relationship [8]. Two criteria that influence the structural formation of MoVO<sub>x</sub> catalyst are the vanadium insertion filling the molybdenum vacancies of the h-MoO<sub>3</sub> structure and followed by vanadium substituting molybdenum. The addition of vanadium affected not only the morphology but

✉ Durga Devi Suppiah  
durgadevi@um.edu.my

<sup>1</sup> Nanotechnology and Catalysis Research Centre (NANOCAT), University of Malaya, Kuala Lumpur, Malaysia

<sup>2</sup> Institute of Research Management and Services (IPPP), University of Malaya, Kuala Lumpur, Malaysia

also the lattice parameters of the molybdenum salt crystal structure [9].

In this paper, the structural properties of molybdenum vanadium oxide-based catalysts were investigated in correlation with temperature and activation condition. In situ XRD analysis was conducted under different activation conditions to reveal the dynamics of structural evolution which helps to determine the active catalyst state. The structural evolution analysis obtained was then correlated with thermal decomposition and heat transfer analysis to further understand the mechanism hence determining the most desirable structure for reactivity studies.

## Experimental

### Synthesis of molybdenum vanadium oxide

Molybdenum vanadium oxides (MoVO<sub>x</sub>) precursor was prepared using sol-gel technique to acquire the desired catalyst structure. This was done by adjusting the method established by Rodel [4]. Firstly 0.1 Mol/L vanadyl oxalate ( $\text{VO}(\text{C}_2\text{O}_4)$ ) solution was prepared by dissolving the vanadium (V) oxide (98% purity) in oxalic acid (98% purity). This was then added to a 0.05 Mol L<sup>-1</sup> solution of ammonium heptamolybdate (AHM, 99%) with the rate of addition of 1 mL min<sup>-1</sup> using an autotitrator at 80 °C. After stirring at this temperature for 1 h, the solution was spray-dried by atomizing with compressed air at 6 bar and dried with hot air at 200 °C using a mini spray-dryer (Buchi). The spray-dried powder was then collected and subjected to thermal analysis and activation followed by structural and morphological characterization.

### In situ X-ray diffraction (in situ XRD) analysis

The structural phase changes with temperature were monitored through an in situ X-ray diffractometer (Bruker) which was equipped with Flowbus mass flow controllers. The spray-dried catalyst precursors were heated from 30 to 500 °C at a heating rate of 5 °C min<sup>-1</sup> under both inert (helium) and synthetic air at 100 mL min<sup>-1</sup>. The diffractograms were obtained using a theta/theta goniometer and a position sensitive detector (PSD). The data sets were collected in the range of  $10^\circ \leq 2\theta \leq 80^\circ$  at 50 °C intervals. Phase analysis was conducted using High Score Plus software. Crystallite size was calculated from the XRD peak broadening using Scherrer equation;

$$\text{Crystallite size } (D) = k\lambda/\beta_{\text{struc}} \cos \theta$$

where  $k$  is the shape factor,  $\lambda$  is the X-ray source wavelength ( $K_{\alpha 1} = 1.541$  nm), and  $\theta$  is the peak position. Peak profile fitting was conducted while the instrumental

broadening was determined using Quartz standard and subsequently subtracted out from the XRD scan.

### Thermal analysis and activation

Thermo-decomposition was analyzed by a Mettler Toledo TGA/SDTA851<sup>e</sup> coupled with a Thermostar Mass Spectrometer (MS) to analyze the evolved decomposition gas as it measures the mass changes with respect to temperature. The MoVO<sub>x</sub> precursor was heated from 30 to 500 °C at a heating rate of 5 °C min<sup>-1</sup> under both synthetic air and also helium at a flow rate of 50 mL min<sup>-1</sup>. The thermograms were evaluated, and the mass loss percentages were determined. The crystallization and melting properties of the precursor were analyzed using differential scanning calorimetry (DSC) technique. The DSC instrument used was a Mettler Toledo DSC822<sup>e</sup> equipped with a measuring cell with ceramic sensors which measures the heat flow to detect endothermic and exothermic effects [10, 11]. All samples were heated from 30 to 500 °C at a heating rate of 10 °C min<sup>-1</sup> under both synthetic air and helium at a flow rate of 50 mL min<sup>-1</sup>. The heat flow/energy of samples was calculated and evaluated. The MoVO<sub>x</sub> spray-dried precursors were then activated under different gaseous environment to investigate the activation effect on the catalyst structural changes. One batch was calcined under static air using muffle furnace (Barnstead Thermolyne) and another batch under helium using Universal Temperature Programmer (UTP) at 500 °C for 4 h.

### Morphological analysis

FEI quanta 200F Field Emission Scanning Electron Microscope (FESEM) was used to investigate the microstructure and surface structural defects of the precursors and the catalyst. The morphology observation was carried out under low vacuum and accelerating voltage of 5.0 HV. The images were captured under magnifications between ranges of 8–30 k. Spot analysis was done using energy-dispersive X-ray (EDX) with INCA energy 400 to quantitatively analyze the local metal content. Elemental mapping was done to verify the metal homogeneity distribution in the MoVO<sub>x</sub> precursors and calcined catalyst.

## Results and discussion

### Catalyst activation analysis via in situ X-ray diffraction

The XRD diffractograms obtained via in situ activation under air (20% Oxygen) are shown in Fig. 1a. The amorphous phase reflection at 12° starts to increase until 250 °C.

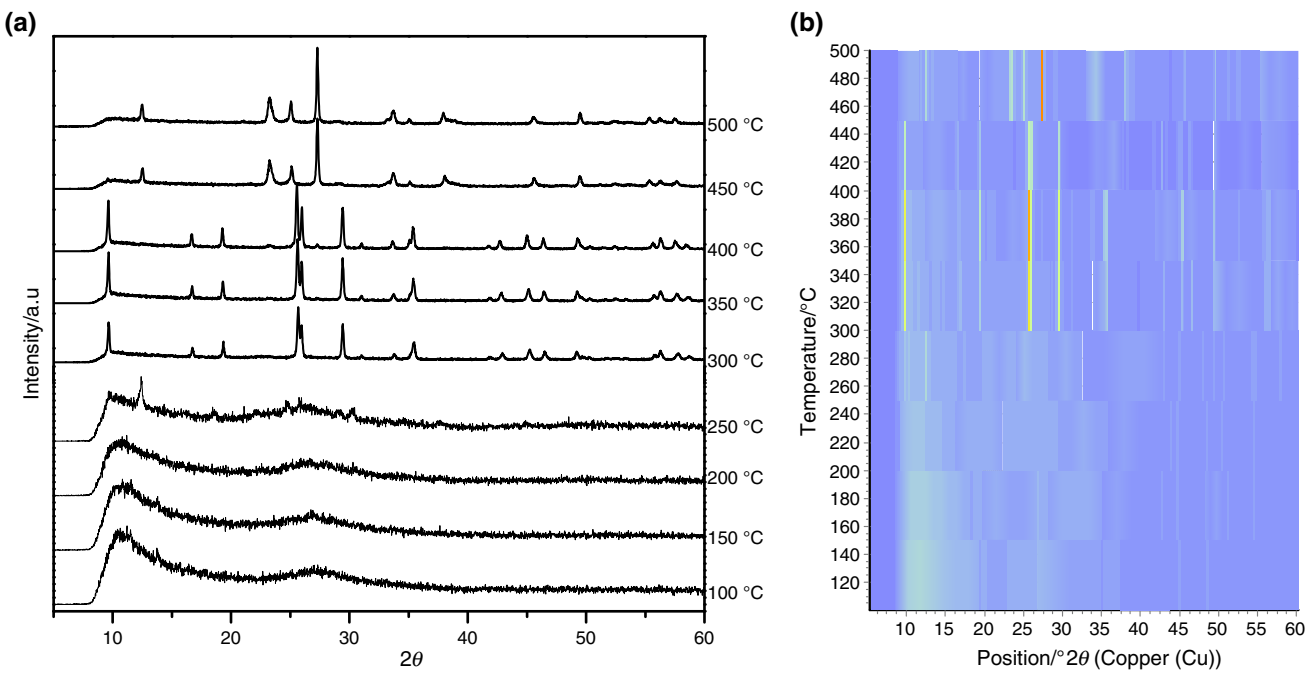


**Fig. 1** **a** In situ XRD. **b** Isoplot of In situ XRD of MoVO<sub>x</sub> precursor activation from 50 to 500 °C under air

At 300 °C, highly crystalline phase was obtained and this can be observed in the thermal Isoplot in Fig. 2b. Analysis of the diffractogram at 400 °C (Table 1) reveals hexagonal crystal structure matching, vanadium molybdenum oxide, Mo<sub>0.87</sub>O<sub>2.94</sub>V<sub>0.13</sub>, (PDF-File 48-0766). The hexagonal structure unit cell volume is 359.39 Å<sup>3</sup> with unit cell parameter  $a = 10.592 \text{ \AA}$ ,  $b = 10.592 \text{ \AA}$ , and  $c = 3.6990 \text{ \AA}$ . This phase maintains until 450 °C.

The phase then changes radically at 450 °C. Analysis of the diffractogram at 500 °C reveals mixed phase structure (Table 2) consisting mainly of orthorhombic phase that correlates with the thermodynamically stable orthorhombic molybdenum oxide, (MoO<sub>3</sub>), (PDF-File 05-0508), which belongs to space group Pbnn (62) with unit cell volume is 202.99 Å<sup>3</sup> with unit cell parameter  $a = 3.962 \text{ \AA}$ ,  $b = 13.858 \text{ \AA}$ , and  $c = 3.697 \text{ \AA}$ . Residue of the hexagonal

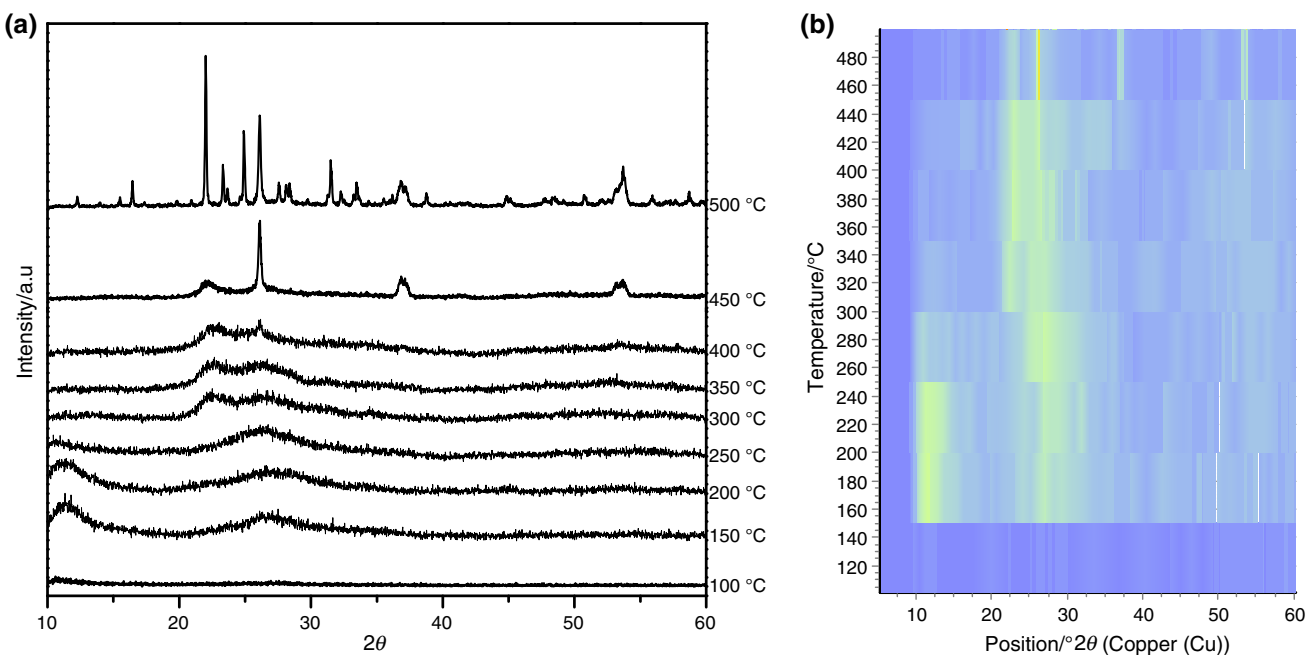


**Fig. 2** **a** In situ XRD. **b** Isoplot of MoVO<sub>x</sub> precursor activation from 50 to 500 °C under helium

**Table 1** X-ray diffraction data of MoVO<sub>x</sub> activation under air (400 °C)

2q	Intensity/%	hkl	<i>d</i> <sub>exp</sub>	<i>d</i> <sub>ref</sub>	Phase
9.60	43.79	100	9.218	9.193	Hexagonal
25.55	100	210	3.483	3.470	Hexagonal
25.98	65.51	101	3.427	3.428	Hexagonal
29.42	35.81	111	3.036	3.033	Hexagonal
35.30	23.47	310	2.543	2.547	Hexagonal

**Table 2** X-ray diffraction data of MoVO<sub>x</sub> activation under air (500 °C)

2q	Intensity/%	hkl	<i>d</i> <sub>exp</sub>	<i>d</i> <sub>ref</sub>	Phase
12.39	24.45	020	6.93	7.13782	Orthorhombic
23.29	64.31	110	3.81	3.81609	Orthorhombic
25.01	37.91	211	3.47	3.55812	Hexagonal
27.2737	100	21	3.26	3.2672	Orthorhombic
33.5763	26.81	220	2.649	2.66693	Hexagonal
38.0356	17.44	131	2.332	2.36388	Orthorhombic

phase still exists. The activation temperature has influenced the crystallite size of the MoVO<sub>x</sub> catalyst. The crystallite sizes were calculated using Scherrer equation as shown in Table 3. The nanostructure crystallite was stabilized by the amorphous matrix attained during the spray drying process [12]. The crystallite size calculated was slightly larger with the structural changes from hexagonal phase (50.6 nm) to orthorhombic phase (55.2 nm). This was because of exposure to air thus causing the complex hexagonal oxides breakdown to the o-MoO<sub>3</sub> phase [13].

The XRD diffractograms obtained via in situ activation under helium are shown in Fig. 2. Similarly, the amorphous phase starts to change at 150 °C with the increase of the highest reflection of the amorphous halo at 12° and 26° regions. These broad amorphous peaks intensities grew with the precursor's degree of crystallinity. The precursor therefore grew in a perpendicular direction along (001) plane which is the reflection of nanocrystalline Mo<sub>5</sub>O<sub>14</sub> [13].

These reflections at 26° continue to increase drastically until 400 °C, while the reflection at 12° reduces and eventually disappears. At this point, it is presumed the

**Table 3** Crystallite size of MoVO<sub>x</sub> after in situ activation under air

Temperature	2θ	FWHM	Crystallite size/nm
400 °C	25.54	0.161	50.6
500 °C	27.27	0.148	55.2

water is removed, leading to the vanadium expulsion into secondary structure which corresponds to an intermediate amorphous form [14]. At 400 °C, crystalline features of the diffractogram appear though the hump is still broad and this is presided to be the nanocrystalline phase of Mo<sub>5</sub>O<sub>14</sub> [15]. Continuous controlled heating of the precursor to 450 °C creates a sharp reflection which is observed at 27°, and this is in good agreement with the domain growth in basal plane [16]. Further heating to 500 °C leads to highly crystalline phase as observed from the thermal Isoplot in Fig. 2b. The final thermodynamically stable phase obtained (Table 4) was vanadium molybdenum oxide (V<sub>0.07</sub>Mo<sub>0.93</sub>)<sub>5</sub>O<sub>14</sub>, PDF-File 31-1437 which corresponds to the tetragonal phase with unit cell volume of 2106.87 Å<sup>3</sup> with unit cell parameter *a* = 22.853 Å, *b* = 22.853 Å and *c* = 4.03 Å. The highly crystalline structure can also be observed in the Isoplot in Fig. 2b. This catalyst can be deduced to having a very high structural stability as temperature does not affect the particles bulk structure which is Mo<sub>5</sub>O<sub>14</sub> which is an advantage of activation under inert gas [16]. The interplanar spacing was larger indicating smaller refined crystallite size due to the confinement of lattice deformations of V<sup>5+</sup> fivefold coordination [17]. The tetragonal structure of Mo<sub>5</sub>O<sub>14</sub> is regarded as a suitable catalyst for alkane activation because of the structure and channel network that can accommodate heteroatom dopants and oxygen for reaction. The structure does not have edge sharing octahedral but instead has clusters of octahedral around a fivefold bipyramidal containing Mo<sup>5+</sup> and V<sup>4+</sup> atoms which are interconnected by a corner-sharing octahedral network consisting of [Mo<sub>8</sub>O<sub>26</sub>]<sup>4-</sup> [18, 19]. In the tetrahedral V<sup>4+</sup> containing groups have oxygen ions which are known to be easier to remove from the lattice during reaction thus promoting the oxygen-containing products. The stability of this catalyst with oxygen vacancies is essential, especially for high dehydrogenation reaction selectivity [20].

According to the Scherrer equation which was calculated using the FWHM value (Table 5), the crystallite size is smaller at the nanocrystalline phase at 450 °C as

**Table 4** X-ray diffraction data of MoVO<sub>x</sub> activation under helium (500 °C)

2θ	Intensity/%	hkl	<i>d</i> <sub>exp</sub>	<i>d</i> <sub>ref</sub>	Phase
16.458	20	330	5.3820	5.3832	Tetragonal
22.017	100	001	4.0340	3.9900	Tetragonal
23.336	28	600	3.8089	3.8065	Tetragonal
24.920	49	540	3.5703	3.5669	Tetragonal
26.105	61	630	3.4107	3.4046	Tetragonal
27.574	18	550	3.2323	3.2299	Tetragonal
31.515	34	740	2.8365	2.8328	Tetragonal

**Table 5** Crystallite size of MoVO<sub>x</sub> after in situ activation under helium

Temperature	2θ	FWHM	Crystallite size/nm
450 °C	26.089	0.250	32.60
500 °C	21.995	0.094	85.80

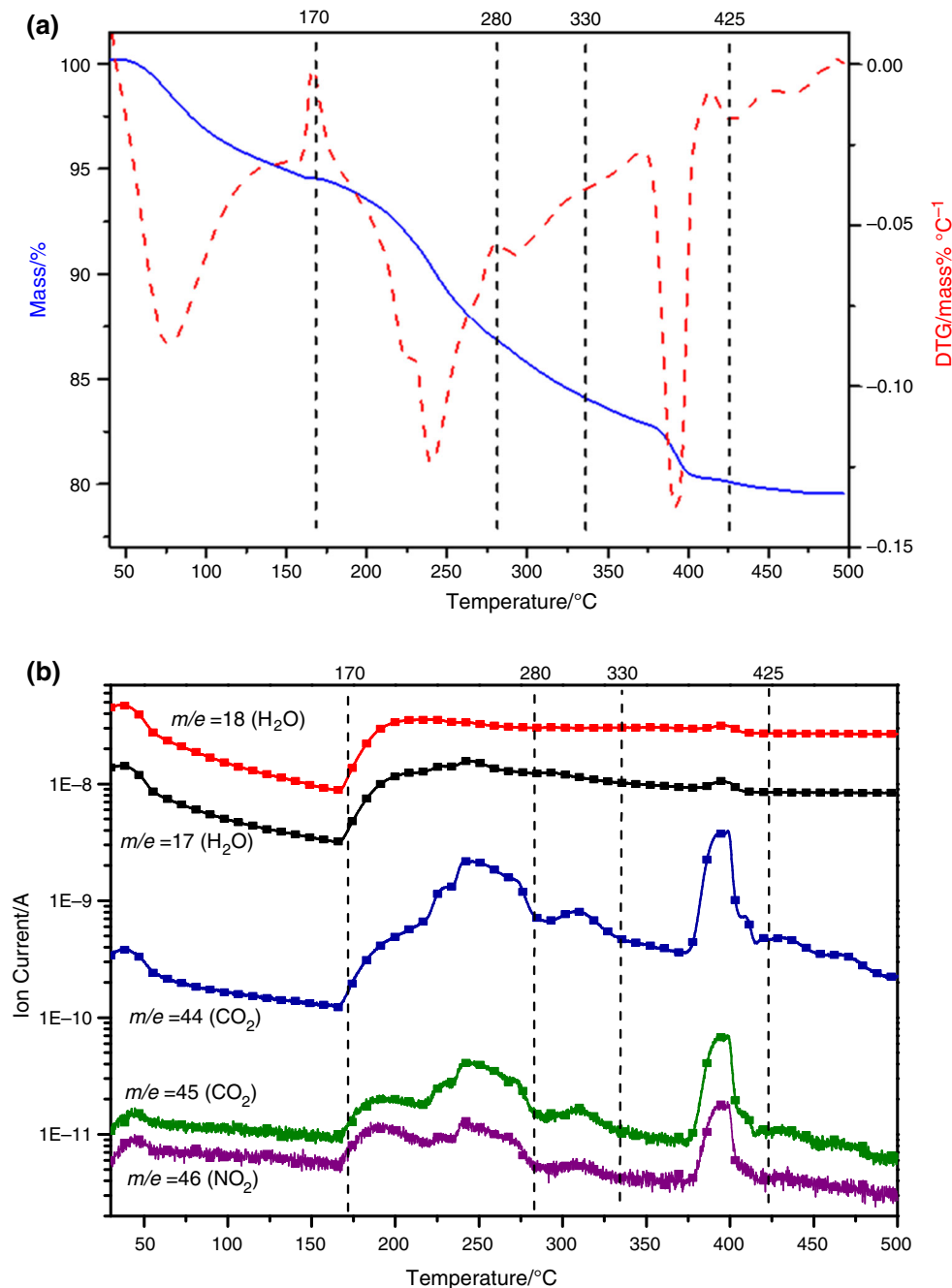
compared to the final tetragonal phase structure at 500 °C. This supports the previous argument that the tetragonal phase growth starts from the nanocrystalline phase at 400 °C and at 500 °C the crystallite size increases in

**Fig. 3** **a** Thermogravimetric analysis. **b** Mass spectrometry analysis of MoVO<sub>x</sub> from 30 to 500 °C under 20 mL air

accordance with particle growth and coarsening of the crystals [21]. As observed, the size which depends on the degree of crystallization varies with different catalyst activation conditions.

### Thermal analysis

In order to further understand the influence of thermal activation condition on the structural changes of MoVO<sub>x</sub>, the synthesized catalyst precursors were subjected to thermal analysis under both activation conditions (static air and helium). The catalyst was subjected to

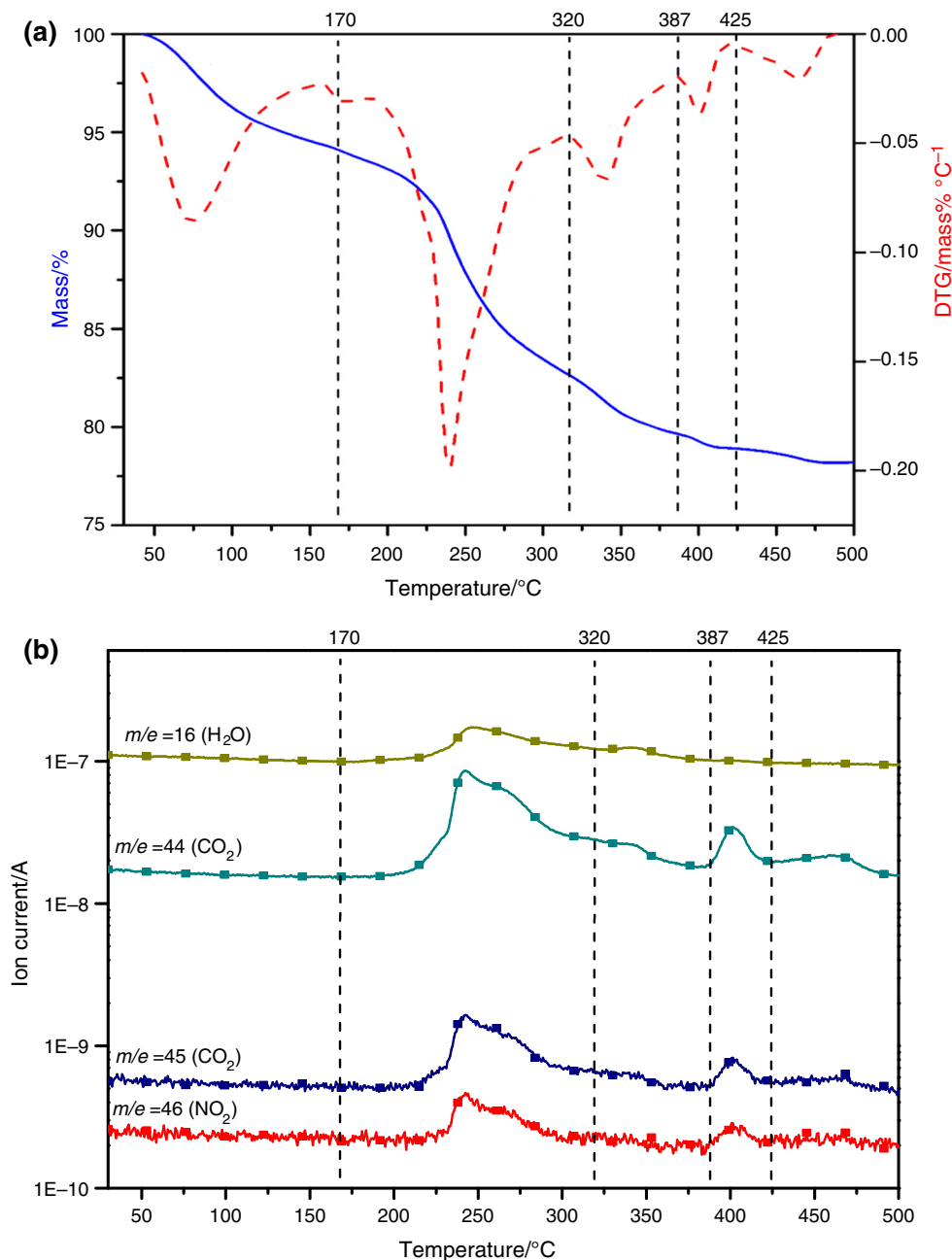


thermogravimetric analysis (TG) accompanied with mass spectrometer (MS) evaluation, and the results were correlated with Differential Scanning Calorimetry (DSC) Analysis.

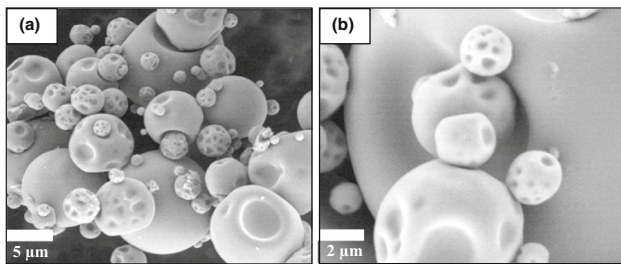
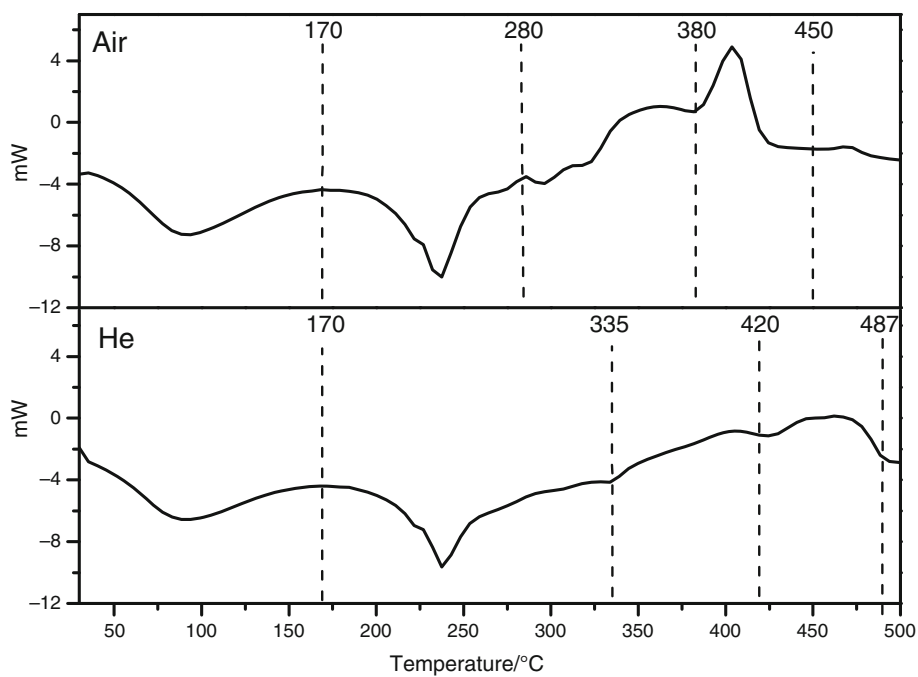
Thermal analysis reveals a complex mechanism of degradation during calcination. Figure 3 shows the TG-MS of MoVO<sub>x</sub> catalyst precursor being activated under 20 mL min<sup>-1</sup> air flow. Four steps of mass loss were recorded. First mass loss of 5.45% was recorded at below 170 °C. Based on the MS evaluation in Fig. 1b, water ( $m/e = 17$  & 18) is released at this point. As the decomposition continues, a second mass loss of 7.68% was recorded

from 170 to 280 °C in the curve involving the desorption of crystallized water ( $m/e = 17$  & 18), carbon dioxide ( $m/e = 44$ ) and nitrogen oxides ( $m/e = 45$  & 46) [22]. The oxidation of ammonia and the reduction of vanadium and molybdenum precursors generate the nitrogen oxides fragments while carbon dioxide formation results from the decomposition of vanadyl oxalate used as the starting material [13]. Similar ion fragments were also observed from the third mass loss of 2.75% from 280 to 330 °C. The final mass loss of 7.3% was recorded at 330–425 °C. At this section, the remaining fragments of water, oxides and ammonium were released as crystallization process to the

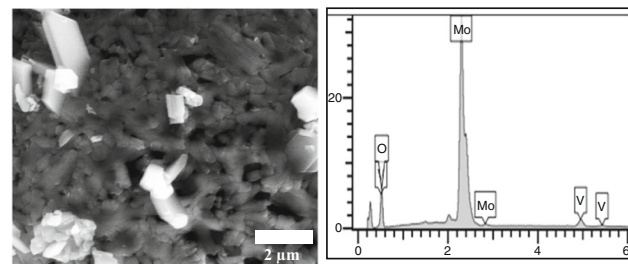
**Fig. 4** **a** Thermogravimetric analysis. **b** Mass spectrometry analysis of MoVO<sub>x</sub> from 30 to 500 °C under 2 0 mL helium



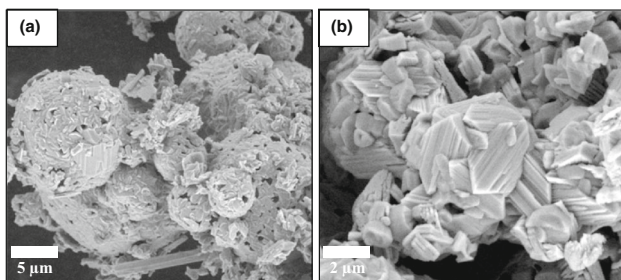
**Fig. 5** DSC plot analysis of MoVO<sub>x</sub> conducted under air and helium



**Fig. 6** SEM image at **a** 8 K. **b** 30 k magnification for MoVO<sub>x</sub> before activation (spray dried)



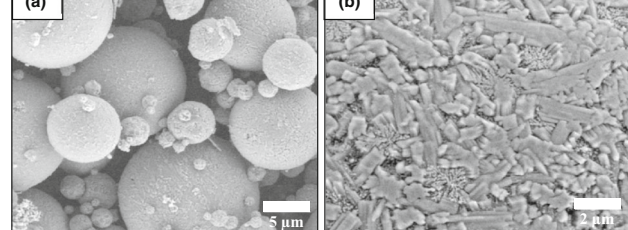
**Fig. 8** Elemental mapping for MoVO<sub>x</sub> (activation under air)



**Fig. 7** SEM image at **a** 8 K. **b** 30 k magnification for MoVO<sub>x</sub> after activation under air

thermodynamically stable tetragonal phase of the catalyst. The huge mass loss recorded was due to exposure to oxidizing medium such as air causes the complex hexagonal oxides breakdown to the o-MoO<sub>3</sub> phase [13].

The curve profile observed in Fig. 4a as the catalyst precursor was being activated under 20 mL min<sup>-1</sup> of helium flow was different from the MoVO<sub>x</sub> catalyst precursor activated under air flow. Five steps of mass loss

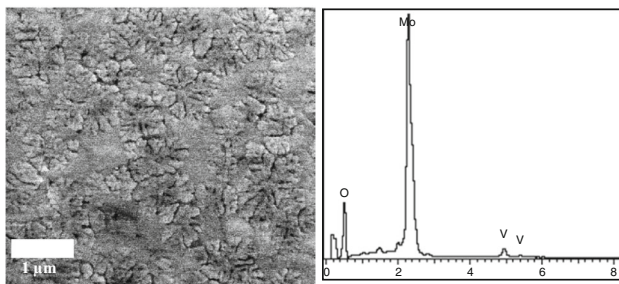


**Fig. 9** SEM image at **a** 8 K. **b** 30 k magnification for MoVO<sub>x</sub> after activation under helium

were recorded. The first mass loss was observed at temperature below 170 °C which corresponds to the loss of water. The largest mass loss (11.64%) was recorded between 170 and 320 °C with the decomposition of mainly carbon dioxide (*m/e* = 44, 45) and nitrogen oxides (*m/e* = 45 & 46) besides desorption of crystallized water (*m/e* = 16). Three more small mass losses were recorded at 320–387 °C (3.15%), 387–425 °C (0.81%) and 425–500 °C (0.47%).

**Table 6** EDX analysis of MoVOx catalyst precursors

Sample	Elements/atomic%		
	Molybdenum (Mo)	Oxygen (O)	Vanadium (V)
MoVOx	16.94	81.86	1.20
MoVOx (activated air)	26.08	71.81	2.12
MoVOx (activated He)	21.40	77.16	1.44

**Fig. 10** Elemental mapping for MoVOx (activation under helium)

The DSC plot shown in Fig. 5 clearly exhibits the calcination condition has influenced the structural properties of the synthesized MoVOx precursor. The first broad endothermic peak observed on both curves corresponds to the release of water as supported by TG–MS evaluation. As the melting process continues, a second endothermic peak is observed which was associated with the second mass loss in the curve, in which the desorption of crystallized water ( $m/e = 17$  & 18) takes place. This curve was broader for MoVOx calcined under helium indicating a slower decomposition of ligands attached to the catalyst precursor.

The bulk nanostructured MoVOx catalyst creates a barrier of heat and mass transfer during activation. Thus, the structural changes were clearly influenced by the degradation temperature. MoVOx degradation temperature under Air was lower than under helium as supported by *in situ* XRD and TG–MS [23]. Oxidative degradation of MoVOx under air catalyst precursor shows an endothermic and exothermic effect at region 280–380 °C whereby it reflects that the melting is leading to the metastable hexagonal phase. A sharp exothermic peak was observed at region 380–450 °C, indicating a major structural changes took place whereby the h-MoO<sub>3</sub> was oxidized to the thermodynamically stable orthorhombic phase (o-MoO<sub>3</sub>). This phase transition is irreversible. However, for DSC curve for MoVOx catalyst precursor which was calcined under helium reveals a higher degradation temperature. Hence, the amorphous structure undergoes two structural changes as shown by the two exothermic peaks

from DSC analysis. A broad exothermic peak was observed above 420 °C indicating crystallization process. This echoes the XRD thermal Isoplot findings whereby the precursor crystallization leads to the thermodynamically stable tetragonal phase (Mo<sub>5</sub>O<sub>14</sub>) of the catalyst [18, 24].

### Microstructures of MoVOx

Figure 6 shows the SEM images of spray-dried MoVOx (a, b) catalyst precursor morphology at 8 and 30 k times magnification. At lower magnification, the images show clusters of spherical, smooth ball-like particles with no discrete features which is consistent with any kind of spray-dried precursors [25]. At higher magnification, the ball-like structure appears to be spherical particles smooth surface areas indicating the effect of drying process on surface texture [26]. However, significant changes can be observed for MoVOx catalytic structure after activation under air flow as shown in Fig. 7a, b. At lower magnification, the ball-like structure appears to be ‘cracked’ and no longer has a smooth surface. At higher magnification, new crystallite structure emerges featuring rough looking hexagonal slices Fig. 8. This confirms the XRD data analysis as shown in Fig. 1 whereby the hexagonal oxides breakdown to the o-MoO<sub>3</sub> phase [13] hence leaving ‘slices’ of the structure. Figure 9a, b show images for MoVOx catalyst precursor after calcination in helium. At lower magnification, the ball-like structure appears to be uneven but less ‘flaky’ unlike images in Fig. 7. At higher magnification, a new finely dispersed phase appears to be compiling finer crystallite. The newly formed particles morphology has long rods of tetragonal cross sections thus further confirming the XRD analysis. Table 6 shows the atomic percentage composition of molybdenum, oxygen and vanadium in the synthesized MoVOx catalyst precursor and calcined samples. Calcination affects the elemental composition with small changes [13]. Based on the elemental mapping analysis in Fig. 8 (MoVOx calcined under air) and Fig. 10 (MoVOx calcined under helium), the elements appear to be highly dispersed in the bulk catalyst surface. There are no aggregates of V<sub>2</sub>O<sub>5</sub> particles which is also supported by XRD analysis [27].

## Conclusions

The understanding of MoVO<sub>x</sub> phase transition during thermo-oxidation (Air) and thermo-degradation (He) is crucial to identify the active phase of the catalyst. Activation under air reveals highly crystalline hexagonal crystal structure at 300 °C. However, at 500 °C, mixed phase consisting mostly the thermodynamically stable orthorhombic molybdenum oxide was obtained. This was in accordance with the thermo-decomposition profile exhibiting an endothermic effect above 380 °C. Activation of MoVO<sub>x</sub> catalyst precursor under helium, however, demonstrates a different trend of crystallization. The structural transformation was from amorphous to nanocrystalline at 400 °C. The crystal growth along the (001) plane indicates the reflection of nanocrystalline Mo<sub>5</sub>O<sub>14</sub>. At 500 °C, the thermodynamically stable tetragonal phase was achieved with high degree of crystallization. All the particles obtained displayed nanocrystalline properties and had been verified by morphology characterization which also showed homogeneous dispersion of the loading metals which provides the ‘site isolation’ effect essential for catalytic propane activation. This dynamics of activation profile provides an insight of the catalyst reactive structural phase which can be further exploited for modified dehydrogenation reaction such as ODH reaction.

**Acknowledgements** The authors would like to thank NANOCAT technical service team for their contribution on sample characterization and ROGS grant scheme (BR010-2014) for providing financial assistance.

## References

- Meunier FC, Yasmeen A, Ross JRH. Oxidative dehydrogenation of propane over molybdenum-containing catalysts. *Catal Today*. 1997;37(1):33–42. doi:[10.1016/s0920-5861\(96\)00253-2](https://doi.org/10.1016/s0920-5861(96)00253-2).
- Cavalleri M, Hermann K, Guimond S, Romanishyn Y, Kuhlenbeck H, Freund HJ. X-ray spectroscopic fingerprints of reactive oxygen sites at the MoO<sub>3</sub>(0 1 0) surface. *Catal Today*. 2007;124(1–2):21–7. doi:[10.1016/j.cattod.2007.01.049](https://doi.org/10.1016/j.cattod.2007.01.049).
- Khan MI, Deb S, Aydemir K, Alwarthan AA, Chattopadhyay S, Miller JT, et al. Vanadium oxide based nanostructured materials for catalytic oxidative dehydrogenation of propane: effect of heterometallic centers on the catalyst performance. *Catal Lett*. 2010;135(3):282–90. doi:[10.1007/s10562-010-0275-6](https://doi.org/10.1007/s10562-010-0275-6).
- Rödel E, Timpe O, Trunschke A, Zenkovets GA, Kryukova GN, Schlägl R, et al. Structure stabilizing effect of tungsten in mixed molybdenum oxides with Mo<sub>5</sub>O<sub>14</sub>-type structure. *Catal Today*. 2007;126(1–2):112–8. doi:[10.1016/j.cattod.2007.03.004](https://doi.org/10.1016/j.cattod.2007.03.004).
- Hu EL, Shaw DT. Synthesis and assembly. In: Siegel RW, Hu E, Roco MC, editors. *Nanostructure science and technology a worldwide study*. Maryland: WTEC, Loyola College; 1999. p. 15–34.
- Koch CC. Nanostructured materials: an overview. In: Zehetbauer MJ, Zhu YT, editors. *Bulk Nanostructured Materials*. Weinheim: WILEY-VCH Verlag GmbH & Co. KGaA; 2009. p. 1–20.
- Bettahar MM, Costentin G, Savary L, Lavalle JC. On the partial oxidation of propane and propylene on mixed metal oxide catalysts. *Appl Catal A Gen*. 1996;145(1–2):1–48. doi:[10.1016/0926-860x\(96\)00138-x](https://doi.org/10.1016/0926-860x(96)00138-x).
- Topsøe H. Developments in operando studies and in situ characterization of heterogeneous catalysts. *J Catal*. 2003;216(1–2):155–64. doi:[10.1016/s0021-9517\(02\)00133-1](https://doi.org/10.1016/s0021-9517(02)00133-1).
- Mougin O, Dubois J-L, Mathieu F, Rousset A. Metastable hexagonal vanadium molybdate study. *J Solid State Chem*. 2000;152(2):353–60. doi:[10.1006/jssc.2000.8663](https://doi.org/10.1006/jssc.2000.8663).
- Wagner M. Thermal analysis in practice. Mettler Toledo collected applications. Schwerzenbach: Mettler-Toledo AG; 2009.
- Gabbott P. A practical introduction to differential scanning calorimetry. In: Gabbott P, editor. *Principles and applications of thermal analysis*. Hoboken: Blackwell Publishing; 2008. p. 1–50.
- Li X, Anton N, Arpagaus C, Belletex F, Vandamme TF. Nanoparticles by spray drying using innovative new technology: the büchi nano spray dryer B-90. *J Controll Release*. 2010;147(2):304–10. doi:[10.1016/j.jconrel.2010.07.113](https://doi.org/10.1016/j.jconrel.2010.07.113).
- Knobl S, Zenkovets GA, Kryukova GN, Ovsitser O, Niemeyer D, Schlägl R, et al. The synthesis and structure of a single-phase, nanocrystalline MoVW mixed-oxide catalyst of the Mo<sub>5</sub>O<sub>14</sub> type. *J Catal*. 2003;215(2):177–87. doi:[10.1016/s0021-9517\(03\)00006-x](https://doi.org/10.1016/s0021-9517(03)00006-x).
- Ilkenhans T, Herzog B, Braun T, Schlägl R. The nature of the active phase in the heteropolyacid catalyst H<sub>4</sub>PvMo<sub>11</sub>O<sub>40</sub>·32H<sub>2</sub>O used for the selective oxidation of isobutyric acid. *J Catal*. 1995;153(2):275–92. doi:[10.1006/jcat.1995.1130](https://doi.org/10.1006/jcat.1995.1130).
- Giebel L, Wirth A, Martens JA, Vogel H, Fuess H. Phase transitions of V-Mo-W mixed oxides during reduction/re-oxidation cycles. *Appl Catal A Gen*. 2010;379(1–2):155–65. doi:[10.1016/j.apcata.2010.03.022](https://doi.org/10.1016/j.apcata.2010.03.022).
- Zenkovets GA, Kryukova GN, Gavrilov VY, Tsybulya SV, Anufrienko VA, Larina TA, et al. The structural genesis of a complex (MoVW)<sub>5</sub>O<sub>14</sub> oxide during thermal treatments and its redox behavior at elevated temperatures. *Mater Chem Phys*. 2007;103(2–3):295–304. doi:[10.1016/j.matchemphys.2007.02.029](https://doi.org/10.1016/j.matchemphys.2007.02.029).
- Dieterle M, Mestl G, Jäger J, Uchida Y, Hibst H, Schlägl R. Mixed molybdenum oxide based partial oxidation catalyst: 2. Combined X-ray diffraction, electron microscopy and Raman investigation of the phase stability of (MoVW)<sub>5</sub>O<sub>14</sub>-type oxides. *J Mol Catal A: Chem*. 2001;174(1–2):169–85. doi:[10.1016/s1381-1169\(01\)00074-7](https://doi.org/10.1016/s1381-1169(01)00074-7).
- Werner H, Timpe O, Herein D, Uchida Y, Pfänder N, Wild U, et al. Relevance of a glassy nanocrystalline state of Mo<sub>4</sub>VO<sub>14</sub> for its action as selective oxidation catalyst. *Catal Lett*. 1997;44(3):153–63. doi:[10.1023/a:1018901830923](https://doi.org/10.1023/a:1018901830923).
- Knobl S, Zenkovets GA, Kryukova GN, Maksimovskaya RI, Larina TV, Vasenin NT, et al. Nanoclusters as precursors to (MoVW)<sub>5</sub>O<sub>14</sub>: in situ and chemical characterisation of the systems of a single phase oxidation catalyst. *Phys Chem Chem Phys*. 2003;5(23):5343–8.
- Mamedov EA, Corberán VC. Oxidative dehydrogenation of lower alkanes on vanadium oxide-based catalysts. The present state of the art and outlooks. *Appl Catal A Gen*. 1995;127(1–2):1–40. doi:[10.1016/0926-860x\(95\)00056-9](https://doi.org/10.1016/0926-860x(95)00056-9).
- Song P, Wang Q, Li J, Yang Z. Morphology-controllable synthesis, characterization and sensing properties of single-crystal molybdenum trioxide. *Sens Actuators B Chem*. 2013;181:620–8. doi:[10.1016/j.snb.2013.02.070](https://doi.org/10.1016/j.snb.2013.02.070).
- Skwarek E, Khalameida S, Janusz W, Sydorchuk V, Konovalova N, Zazhigalov V, et al. Influence of mechanochemical activation on structure and some properties of mixed vanadium–molybdenum oxides. *J Thermal Anal Calorim*. 2011;106(3):881–94. doi:[10.1007/s10973-011-1744-x](https://doi.org/10.1007/s10973-011-1744-x).

23. Mojtabaei A, Otadi M, Goodarzi V, Khonakdar HA, Jafari SH, Reuter U, et al. Influence of fullerene-like tungsten disulfide (IF-WS<sub>2</sub>) nanoparticles on thermal and dynamic mechanical properties of PP/EVA blends: correlation with microstructure. Compos Part B Eng. 2017;111:74–82. doi:[10.1016/j.compositesb.2016.12.006](https://doi.org/10.1016/j.compositesb.2016.12.006).
24. Zakharova GS, Volkov VL, Täschner C, Hellmann I, Klingeler R, Leonhardt A, et al. Synthesis, characterization and magnetic properties of hexagonal (VO)0.09V0.18Mo0.82O<sub>3</sub> 0.54H<sub>2</sub>O microrods. Mater Lett. 2011;65(3):579–82. doi:[10.1016/j.matlet.2010.11.001](https://doi.org/10.1016/j.matlet.2010.11.001).
25. Kunert J, Drochner A, Ott J, Vogel H, Fueß H. Synthesis of Mo/V mixed oxide catalysts via crystallisation and spray drying—a novel approach for controlled preparation of acrolein to acrylic acid catalysts. Appl Catal A Gen. 2004;269(1–2):53–61. doi:[10.1016/j.apcata.2004.03.050](https://doi.org/10.1016/j.apcata.2004.03.050).
26. Endres S, Kampe P, Kunert J, Drochner A, Vogel H. The influence of tungsten on structure and activity of Mo-V-W-mixed oxide catalysts for acrolein oxidation. Appl Catal A Gen. 2007;325(2):237–43. doi:[10.1016/j.apcata.2007.02.040](https://doi.org/10.1016/j.apcata.2007.02.040).
27. Cha W, Chin S, Park E, Yun S-T, Jurng J. Effect of V<sub>2</sub>O<sub>5</sub> loading of V<sub>2</sub>O<sub>5</sub>/TiO<sub>2</sub> catalysts prepared via CVC and impregnation methods on NO<sub>x</sub> removal. Appl Catal B Environ. 2013;140–141:708–15. doi:[10.1016/j.apcatb.2013.05.002](https://doi.org/10.1016/j.apcatb.2013.05.002).